Electronic Supplementary Material (ESI) for Lab on a Chip.

Supplementary Information

Microfluidic in-line Dynamic Light Scattering with a Commercial Fibre Optic System

Luis M. G. Torquato[a], Nelson Hélaine[b], Yufan Cui[a], Róisín A. O'Connell[a], Jérémie Gummel[c], Eric S.J. Robles[d], David Jacob[e], and João T. Cabral[a, *]

[a] Department of Chemical Engineering, Imperial College London, London, SW7 2AZ
[b] CNRS UMR 5623, Laboratoire des IMRCP, Université Paul Sabatier, Toulouse, France
[c] Procter & Gamble, Brussels Innovation Centre, Temselaan 100, 1853 Strombeek-Bever, Belgium
[d] Procter & Gamble, Newcastle Innovation Centre, Newcastle upon Tyne NE12 9TS, United Kingdom.
[e] Cordouan Technologies, 11 Avenue Canteranne, 33600 Pessac, France
[*] j.cabral@imperial.ac.uk

1 Flow-DLS setup: capillary and microfluidic systems

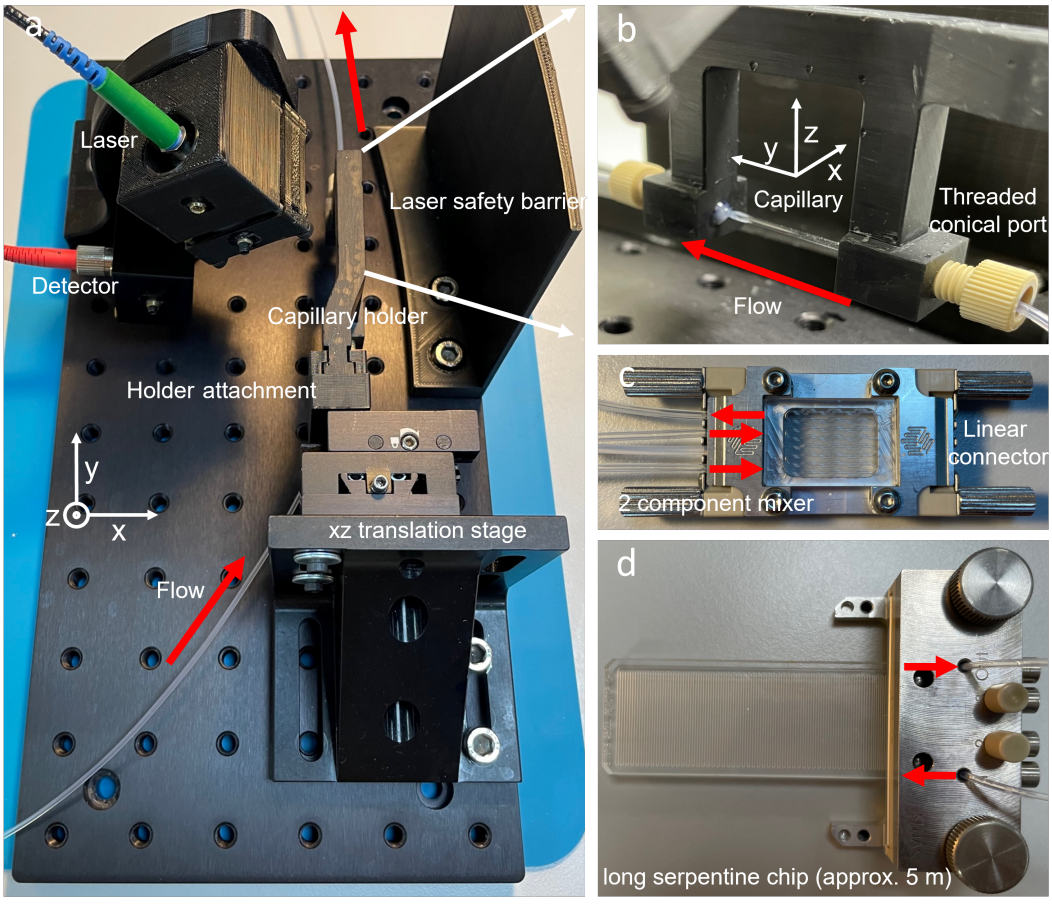

Figure S1. a) Custom capillary-DLS setup. The fibre optic laser and detector are mechanically aligned to the same plane, while the 3D printed capillary holder is aligned using the xz translation stage. b) A close up of the microfluidic fittings and capillary in the holder. o-rings are used to seal the connection between the 3D printed part and the threaded conical port (Idex Flangeless Fitting, Cole-Parmer UY-02020-76). c) Microfluidic mixer used in the ramp experiments, whose output connects onto the capillary. d) Microreactor chip used for direct DLS measurements where the optics were aligned with a single channel.

Various aspects of our experimental setup are depicted in Fig. S1 and were used in different arrangements throughout this work:
(i) For quiescent measurements, a pump was connected directly onto the FEP tubing to fill up the capillary; flow was switched off and measurements were carried out on the filled capillary as shown in figure S1a-b.
(ii) For under flow measurements, the solution was displaced at a constant flow rate, after a $\sim$ 10 s stabilisation time to ensure steady-state flow conditions.
(iii) Measurements on capillaries of ID = 0.4 and 0.2 nm were carried out with the setup and procedure in (i) using different 3D printed capillary holders.
(iv) For direct measurements on the microfluidic chip (Fig. S1d), the $\approx$ 5 m long serpentine channel was filled, and the rectangular glass chip was secured to another 3D printed holder and a single channel was aligned with the optics using the xz-transition stage. Subsequently, measurements were carried out under quiescent conditions.
(v) For the composition ramp experiments, 2 pumps were connected to the inputs of the micromixer chip in Fig. S1c using the 4-way linear connector shown, with one of the inputs blocked. The output of the chip was then connected via the FEP tubing to the capillary in Fig. S1a-b and measurements were taken under flow with changing composition.

2 Beam dimensions

Beam profile measurements were carried out using a Beamage-3.0 beam profiling camera, to extract both the beam waist ($1/e^2$) and the full width half maximum (FWHM) diameter, both shown in Fig. S2. The data agree well with our calculated value of 25 μm for the beam radius, w from the transit correlation function, using the model solutions or dispersions as secondary calibration standards.

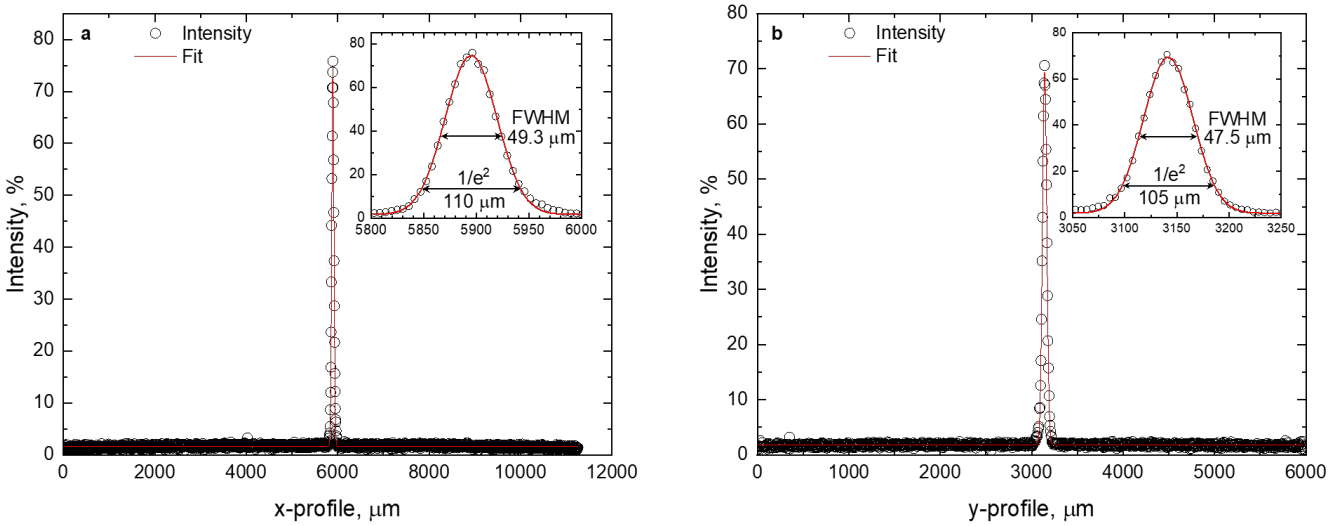

Figure S2. The X-profile (a) and Y-profile (b) of the incident laser beam used in our setup. A Gaussian fit was implemented to determine the FWHM diameter and the beam waist ($1/e^2$).

3 Concentration limits of DLS measurements

Measurements were carried out to estimate the lower concentration limit for detection in a the fiber optic capillary setup (and benchmarked against a Malvern Zetasizer for comparison). We selected the DDAD surfactant system as it forms micelles of small dimensions ($\sim$5 nm), and has a refractive index of $\sim$1.376 making it a challenging system to test the detection limits of our DLS setup. Figure S3 shows that our fibre optic system is sensitive down to the critical micelle concentration (CMC) of this system, namely $\sim$ 0.02% w/w. These values are commensurate with the results of a conventional 'sizer', such as the Malvern Zetasizer, also included in the figure. In practical terms, capillaries or microchannels of greater dimensions provide more robust measurements, likely due to the ease of alignment of the illuminated volume within the cross-section.

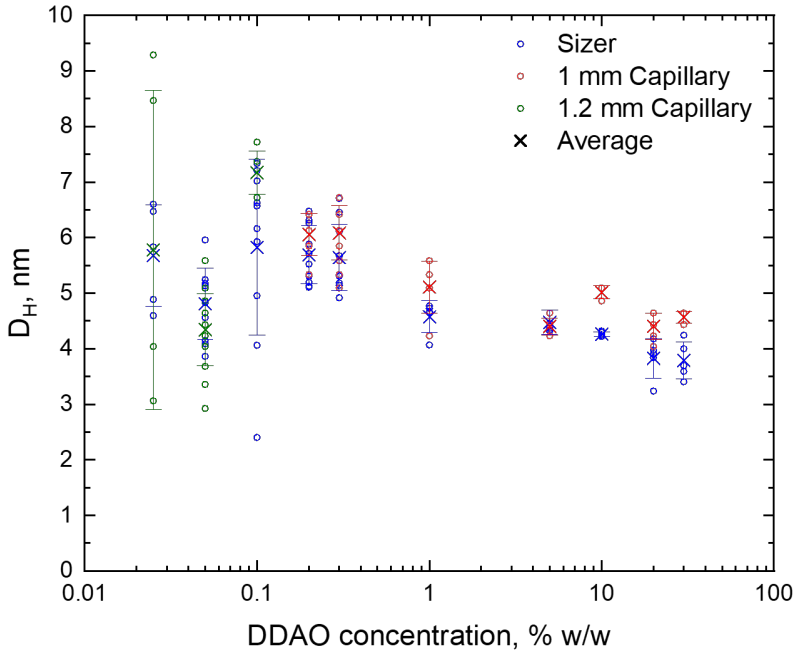

Figure S3. Measurements of D_H ($\circ$) and the average mean value ($\times$) for DDAO solutions of different concentrations from the Malvern Zetasizer (Sizer) and the fiber optic capillary setup with capillaries of different diameters. The error bars display the standard deviation.

4 Measurement time analysis

The evolution of fitting parameters with sampling time (corresponding to the time taken to collect scattering data), agree well with the magnitude of fluctuations of the extracted R_H values shown in Fig. 4 of the main paper. From these data combined, we estimate that ~ 3 s is the minimum measurement time appropriate for a 1% w/w DDAO solution in water to acquire sufficient statistics, estimated from the broad invariance of χ^2 or R^2 beyond this sampling time. This minimum time, however, will dependent on the specific system, including size, refractive index contrast with the solvent, concentration of particles, scattering angle, etc. However, our demonstration using 1% w/w DDAO/H_2O can be considered as a benchmark low-scattering system due to a similar refractive index to water and small micelle sizes, and we have thus employed 3 s as a reasonable minimum time for all other systems investigated.

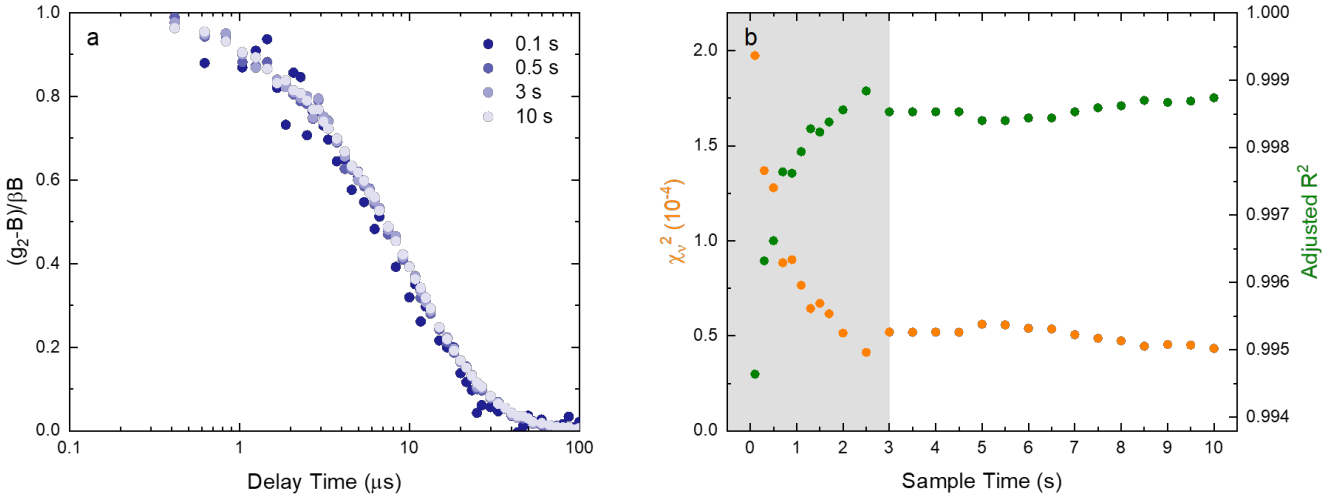

Figure S4. a) Correlograms obtained for different sampling times of a 1% DDAO aqueous solution. b) Evolution of the reduced χ_v^2 and adjusted R^2 associated with fitting $g_2 = B\left(1+\beta e^{-2\Gamma\tau}\right)$ to the correlograms at different sample times. Above ~ 3 s sampling time, the quality of fits remains largely unchanged, in agreement with Fig. 4 of the main paper. we take this as an estimate for minimum integration time for our system to ensure robust R_H estimates.

5 Modified Correlation Function (MCF)

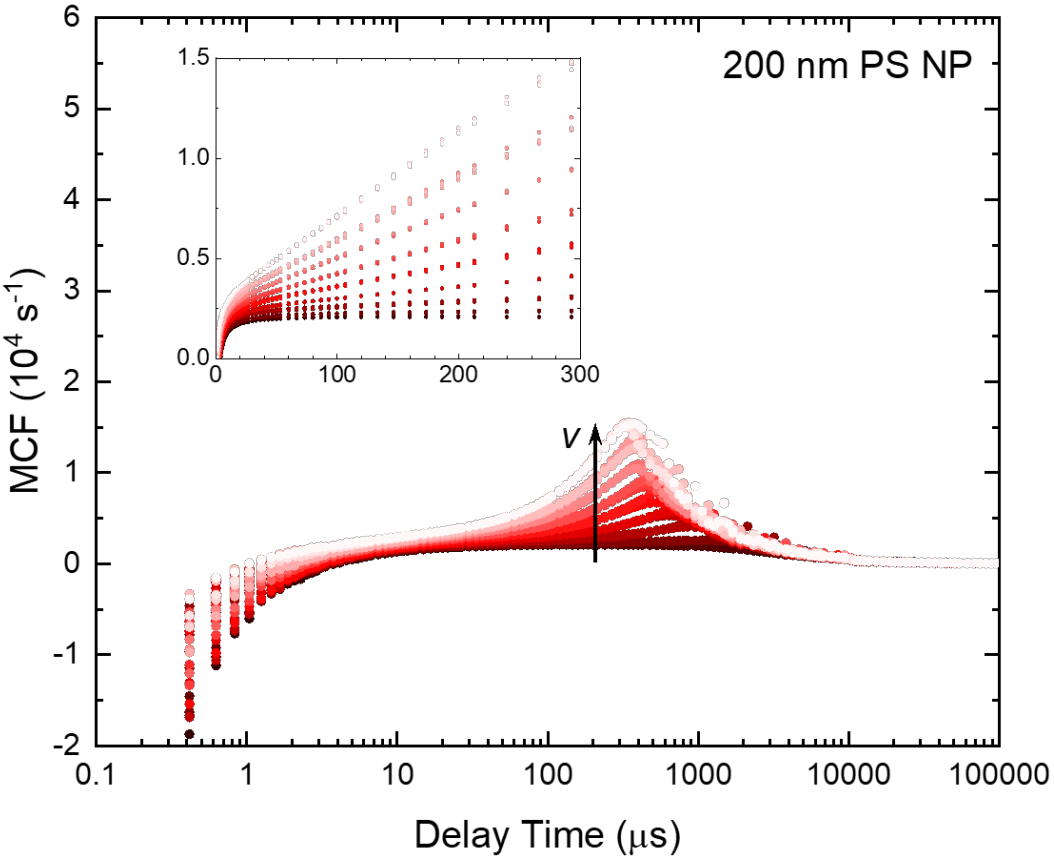

Figure S5. Correlation functions in the MCF rearrangement over the whole range of delay times (in log scale) and linear scale near the region of linearity (inset).

From the rearrangement of the modified correlation function shown in Eq. 9 of the main paper, one could *incorrectly* assume that the correlograms are transformed to a linear function over the full range of delay times. This is absolutely not the case, as shown in Fig. S5, and strong deviations are observed for 'sufficiently low' or 'high' delay times.
Mathematically, the explanation for this is due to the normalised g_2 correlation function being ≈ 1 for low delay times and ≈ 0 at high delay times, while the MCF is proportional to $1/\tau$. In these regions, where the normalised correlation function is approximately constant, but the delay time is changing by orders of magnitude, the dependence on $1/\tau$ dominates. By carefully considering the full MCF profile, we observe that the function is only linear in the region where g_2 is decaying significantly, i.e. for delay times close to where $g_2 \approx 0.5$. For this reason, we have therefore decided to follow a simple, yet robust procedure of only fitting the MCF to data points corresponding to $0.2 > (g_2 - B)/B\beta > 0.8$ where the MCF follows the expected linear relation. This criterion was validated for different v and R_H in the main paper.

6 SEM of polystyrene nanoparticles

In order to determine the actual size of PS NP without relying solely on the manufacturer-provided 'nominal' dimension (obtained by the use of a CPS DISC Centrifuge 24000), SEM was carried out on PS NP of various size ranges.

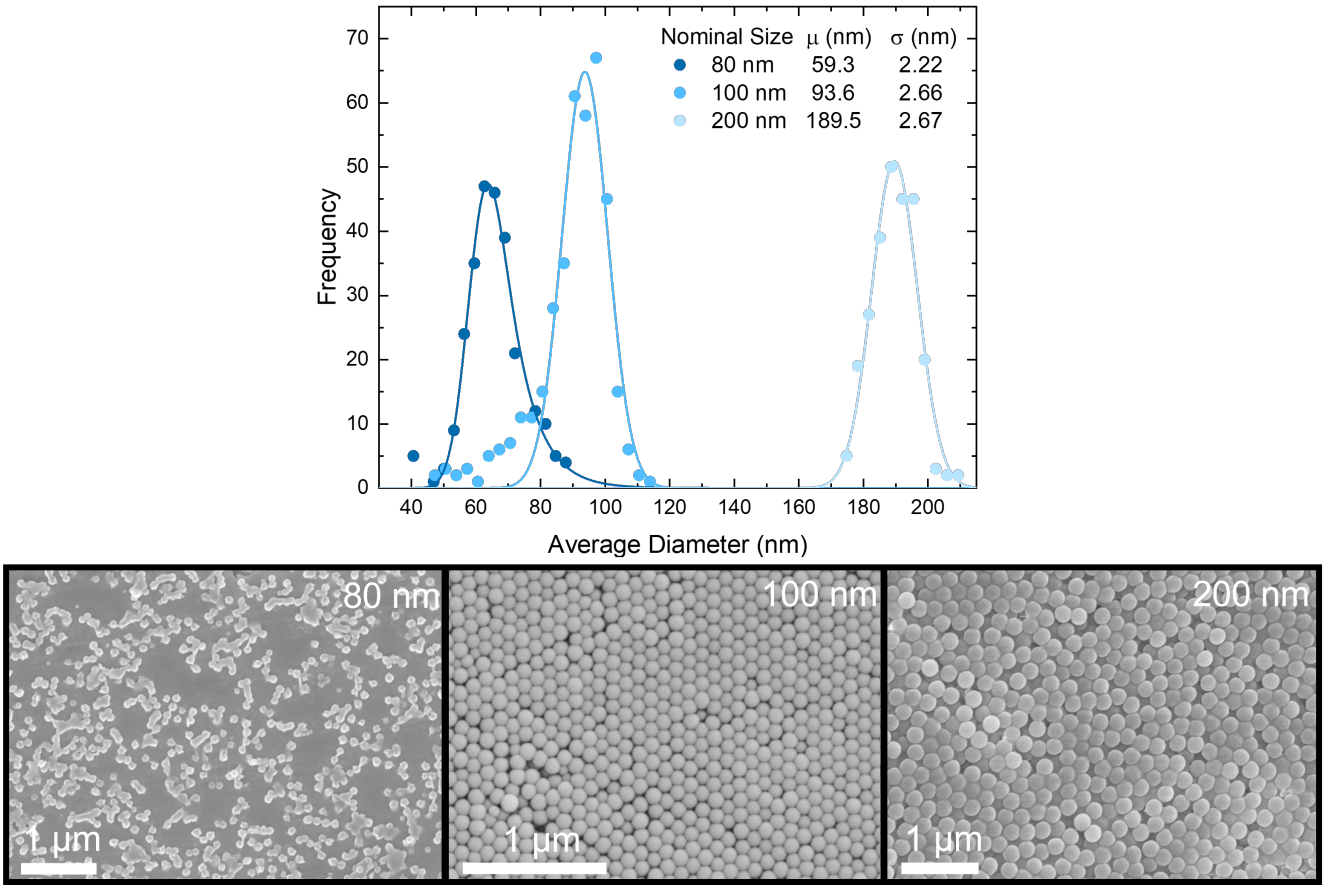

Figure S6. Histograms showing the distribution of diameters of 80, 100, and 200 nm (nominal) PS NPs obtained from processing the SEM data shown in ImageJ using the particle analyser tool and accounting for the thickness of the gold coating on the particles. The histograms were fitted with a normalised Gaussian distribution and the mean diameter and standard deviations are given. By cross-referencing these diameters with the measured R_H values for the systems, there is a reasonably good agreement between the two experimental methods.

7 Variation of Flow-DLS analysis limits with system properties

The map provided in Fig 8 of the main paper provides estimates for boundaries of applicable data analysis procedures for flow-DLS. The map was computed with the set of parameters for the system, namely scattering angle $\theta = 130°$, laser wavelength $\lambda = 638$ nm, temperature T = 25° C, solvent refractive index $n = 1.33$, and viscosity $\eta = 8.9 \times 10^{-4}$ Pa.s (water), as well as beam radius $\omega = 25\ \mu$m. While the main results of the map hold in general, here we adjust the estimates for different, plausible, system parameters. For clarity, we provide only the boundary between the range where the MCF approach holds, and the region where deviations become pronounced and cannot be modelled by the theory. This corresponds to the boundary between the light green ('transit theory') and orange ('deviations') ranges of Fig. 8 of the main paper modeled by $v = 2Dq^2\omega \propto 1/R_H$ and $g_{2,T} \approx 0.75$.

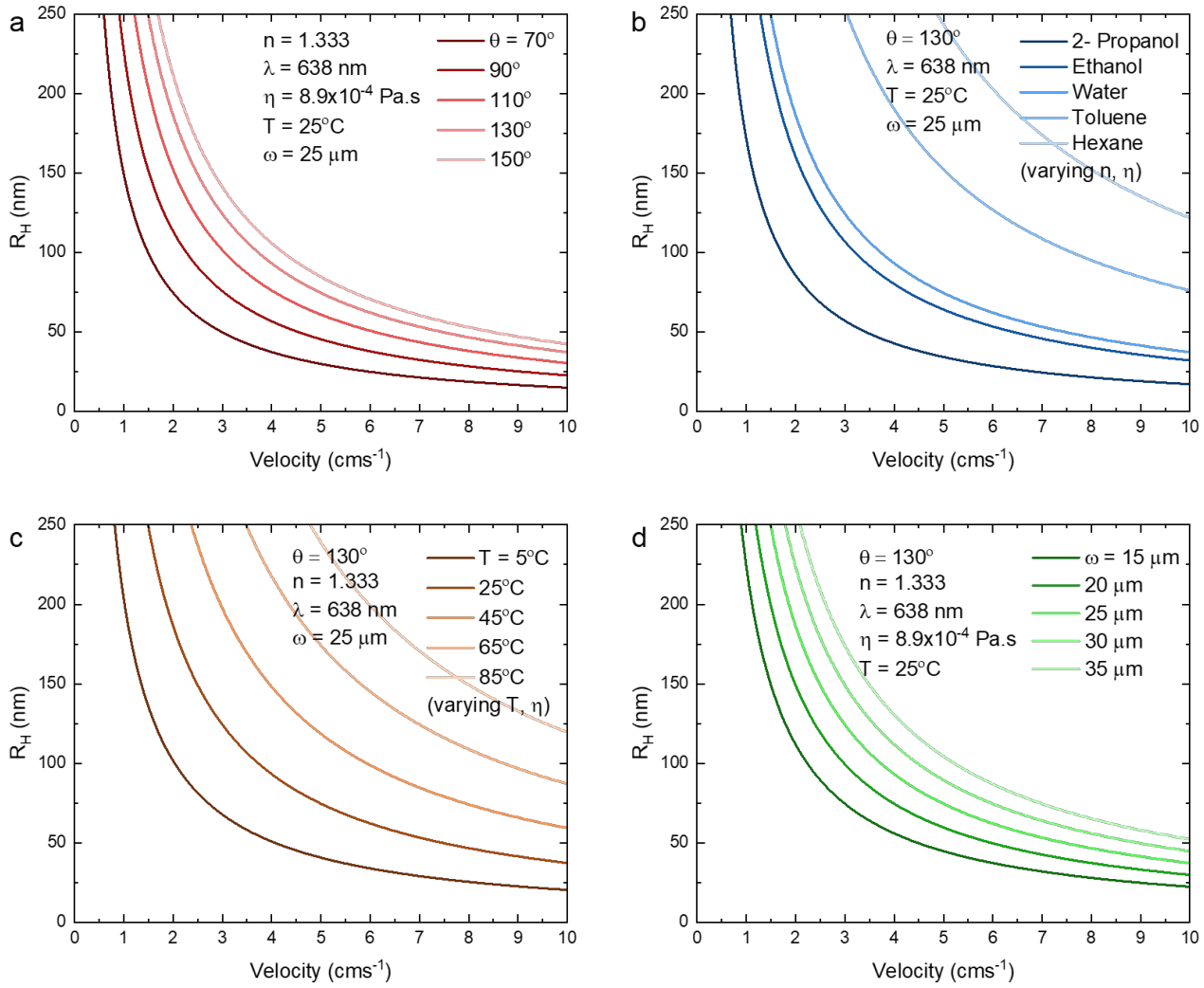

Figure S7. Effect of (a) scattering angle, (b) solvent properties (including changes in refractive index and viscosity), (c) temperature, and (d) beam radius, on the estimated boundary between transit-DLS theory being applicable and deviations from invariant R_H with increasing v behvaviour.

The boundaries between the 'transit DLS' and 'deviation' regimes are based on the proportionality between $v = 2Dq^2\omega \propto 1/R_H$, arising from the relative magnitudes of the Brownian and transit terms. The boundaries therefore shift to higher velocities by increasing the scattering angle (Fig. S7a) and thus increasing q; or by a lower viscosity of the medium (the main contribution in Fig. S7b) increasing the value of the diffusion coefficient, D; or increasing the temperature and thus simultaneously reducing the viscosity (Fig. S7c); or by increasing the beam width ω (Fig. S7d).

The dependence of the regime boundaries with experimental parameters can be understood, in simple terms, as follows. While it is trivial that correlograms shift with angle, when measuring particles of the *same* size due to the intrinsic dependence of $\Gamma = Dq^2$ in wavenumber q (and thus angle θ), given $D_H \propto 1/R_H$, the size-dependence of the decorrelation time also results in slightly different boundaries when compared against the transit term.

Modifications to the DLS setup may be carried out to expand the v-R_H parameter space where the transit correlation function holds, namely by increasing the scattering angle, using solvents of lower viscosities, or increasing the beam width. The latter, however, imposes greater constraints on the azimuthal angle between the wavevector and perpendicular to the velocity (expressed in Eq. 6), and an increase in the shear rate gradient in the scattering volume that also increases the constraint on the azimuthal angle, and hence shear correlation function models may need to be considered. Increasing the scattering angle would alleviate restrictions on the azimuthal angle (Eq. 6), and widen the region of applicability for transit theory. However, in our setup, a reduction in the spacial coherence factor, β, was observed, indicating a tension between data quality and increasing the v-R_H parameter space where theory applies.

8 Impact of capillary and microchannel dimensions

One of the benefits of our proposed flow-DLS setup, employing a fibre optic, contact-free arrangement, is the ease in changing the flow cell for different measurements and applications, which only requires the design and printing of new holders. Figure S8 shows the data obtained within different flow cells: capillaries with reduced ID from 1 mm to 0.4 and 0.2 mm shown in Fig. S8a, and direct measurements on a microchannel of a microfluidic deviced shown in Fig. S1d, with data shown in Fig. S8b. Illustrative data were collected for both 3% w/w DDAO and 0.01% v/v 100 nm PS NP (nominal size) samples under quiescent conditions.

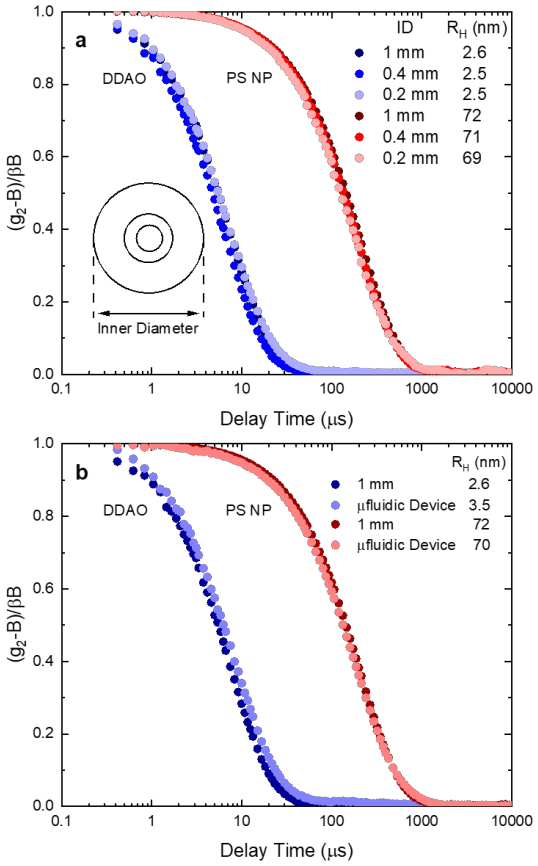

Figure S8. Normalised correlograms acquired for 3% w/w DDAO (blue) and 0.01% v/v PS NP of 100 nm (nominal, red) in water, measured in (a) capillaries of internal diameters 1, 0.4, and 0.2 mm under quiescent conditions, and (b) in a microfluidic channel of cross-section 250 μm depth $\times$ 400 μm width compared to correlograms obtained within a 1 mm capillary under quiescent conditions.

The correlograms and extracted R_H values for the ID reduction experiments are commensurate within the repeatability error of the instrument, suggesting that a reduction in the flow cell dimensions is feasible, if required/beneficial. Furthermore, the direct measurement on the microfluidic channel also showed consistent data with measurements on the 1 mm capillary for the PS NP sample. For measurements on DDAO micellar solutions, we observe an apparent increase of $\sim$0.9 nm in R_H. We believe this could be due to two things: interference between incident and scattered light from the flat surface of the chip leading to a change in the scattering angle and hence wavevector that was not accounted for by the correlator, and the misalignment of the optics on the channel and potential clipping of the curved channel walls leading to parasitic scattering. The former would need to be accounted for on a case by case basis depending on the microdevice, while the latter could be remedied by designing a holder specifically for the dimensions and alignment required for the chip.

9 Apparent hydrodynamic radius of SDS micelles

Size measurements of particle dispersions and solutions by DLS generally assume dilute and weakly interactions conditions, as crowding effects or strong interactions cause departures in the Brownian models for analysis, which is thus replaced by appropriate models. Measurements of SDS micelles in Fig. 9d show an apparent R_H of $\sim$0.5 nm at 0.4 M (10% w/w) SDS and $\sim$10 mM NaCl. This apparent R_H does not correspond to the actual micellar dimensions and is impacted by electrostatic effects discussed in the main paper. In short, these increase the diffusion coefficient which then appears as a lower R_H in the Stokes-Einstein framework. At sufficiently low SDS concentrations, the apparent R_H becomes the actual R_H as shown in Fig. S9. Addition of electrolytes can thus mitigate these additional contributions, providing a means to recovering actual R_H, albeit other structural changes can be inadvertently caused. Since DDAO is a non-ionic (amphoteric) surfactant, this effects are not observed in this system, as seen in Fig. S3 and S8.

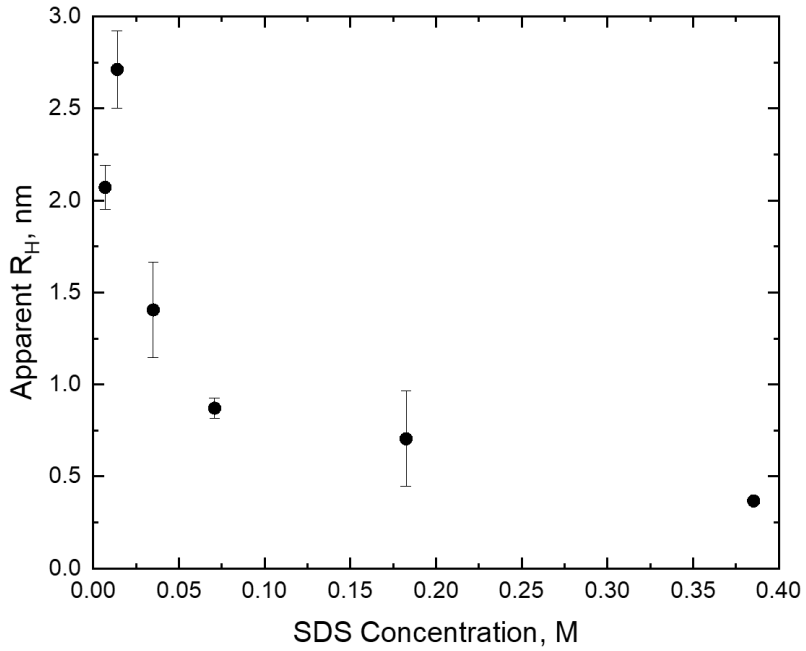

Figure S9. Apparent R_H of SDS micelles with concentration, measurements taken with a Malvern Zetasizer.

10 Towards an automated procedure for data analysis

In this section, we outline the sequence of steps which would enable a non-expert user, or indeed an automated analysis routine, to use the fibre-optic DLS setup described in the main paper, employing a capillary or microchannel device.

1. Run the measurement under flow and obtain the intensity correlation function, g_2, and normalise using the background, B, and spatial coherence factor, β.
2. From the normalised correlogram g_2, Textract the correlation time interval corresponding g_2=0.8 and g_2=0.2.
3. Convert the intensity correlation function g_2 into the MCF representation, using Eq. 9 of the main paper.
4. Fit a straight line to the MCF within the correlation time interval defined in step 2.
5. From the intercept value ($2\Gamma = 2Dq^2$) calculate R_H, and from the gradient (v^2/ω^2) calculate the flow velocity, v. The corresponding equations are also illustrated in Fig. 5b of the main paper.
6. Use the criteria established in Fig. 8a to check the approximate region for the measurement.
7. If the data appear within the deviations or breakdown regions of Fig. 8a, it is recommended to reduce the flow rate (or equivalently increase capillary/microchannel diameter) to bring the measurement into the 'green' regions.